Vibration energy harvesting for cars: semi-active piezo controllers

On behalf of all authors, the corresponding author states that there is no conflict of interest.

G. Pepe[1], A. Doria [2], N. Roveri[1], A. Carcaterra [1]
[1]Department Of Mechanical and Aerospace Engineering, Sapienza University of Rome
[2]Department of Industrial Engineering, University of Padova
Email: gianluca.pepe@uniroma1.it, alberto.doria@unipd.it, nicola.roveri@uniroma1.it, antonio.carcaterra@uniroma1.it

ABSTRACT:
Energy harvesting represents one of the recent challenging subjects related to vibration and control. The scale of energy harvesters and storage can involve a wide power range but the micro and mesoscale range up to some Watts is the elective field of piezoelectric applications. This paper investigates the power frontiers of the piezoelectric based harvesters applied to automotive units. The analysis, using also experimental data, is aimed at estimating the upper bound of the specific power of this technology for powering small devices on board cars. This paper compares passive optimally tuned piezoelectric harvester and semi-active controlled ones, based on a new control strategy named VFC-Variational Feedback Control, recently developed by the authors. This new technique makes it possible to increase in a significant manner the total energy storage drained from car vibrations. Numerical simulations of the new circuitry based on experimental vibration data show the harvester performances of the new device.

KEYWORDS: Energy Harvesting, Car Vibrations, Piezoelectric, Optimal Control Theory, Variational Control, Nonlinear Control.

1. INTRODUCTION

Nowadays piezoelectric devices are widely used for scavenging energy from ambient vibrations. The main advantages of piezoelectric materials in energy harvesting stand in the large power density and the no need for external power sources.

Several studies have investigated the power output of a harvester excited by a fixed frequency vibration source. The results show, as intuitive, the generated power can be maximized when the natural frequency of the harvester is tuned on the vibration frequency and when the electrical load is set to an optimum value [1, 2]. Both experimental and numerical results [3] have revealed the existence of two characteristic natural frequencies related to the harvester, one is the short circuit resonance frequency, the other is the open circuit natural frequency. The difference between these frequencies becomes important when the electromechanical coupling coefficient is large [4]. Optimal values of a purely resistive load that maximizes power output at the two typical resonances can be found in [3]. Some researchers extended the investigation considering more realistic electrical loads, which include the AC-DC converter [4-6]. In this case, optimal values of the load impedance can maximize the power output.

These analyses show that a suitable variation of the load impedance can compensate for the decrease in the generated power when the excitation frequency moves away from the resonance condition. Hence, it is possible to collect a relevant amount of power in the frequency bandwidth about the resonances [7].

The performance of a simple passive harvester with a given load impedance is poor when the source of excitation is characterized by broadband and/or variable spectrum. Sources like these are rather common in many engineering systems. In vehicles, the spectrum of vibrations caused by tire-road interaction and by the engine forces shows many components changing in time, because of the different engine/motor rotational speed variations and the different road roughness [8]. In large structures (e.g. bridges and buildings) vibrations due to traffic and to wind have broadband and variable spectra [9].

Two approaches have been proposed to improve the power output of piezo harvesters in the presence of broadband and/or variable spectra. The first approach consists of widening the band of operation of the passive harvester modifying the mechanical sub-system. Many solutions have been proposed in recent years [10] and they are based on harvester arrays [11-13], trimming devices [14], complex harvester geometries [1, 15-17], and on the exploitations of nonlinear effects [18-23].

The second approach consists of the development of harvesters equipped with adaptive circuits, which take into account the vibration spectrum and can modify their load impedance [7]. An adaptive AC-DC rectifier, able to adjust the output voltage according to the vibration amplitude, is described in [24], to achieve the maximum power transfer. A good review of adaptive circuits for maximizing power output is presented in [25]. Recently, some active circuits are designed to increase both the generated power and frequency bandwidth. In particular, in [26], a tunable synchronous electric charge extraction interface is illustrated. It increases the frequency bandwidth about the resonance in which a significant amount of power can be harvested. In [27], a power processing circuit, equipped with an artificial neural network, can set the impedance connected to the harvester to its optimum value.

In this paper, the energy harvested by a cantilever piezo harvester installed in a car is boosted by employing a new controller based on the Variational Feedback Control (VFC) strategy. VFC controllers have been recently used to improve the performance of semi-active car suspensions [28-30] and to control other complex systems [31-34]. The potentialities of this control strategy in the field of vibration energy harvesting have been highlighted in [35], which adopted a general approach suited to electromagnetic, piezoelectric, and capacitive harvesting.

This paper is organized as follows. The mathematical model of a cantilever piezoelectric harvester is presented in Section 2. The equation of motion is solved with the modal decomposition approach and the maximum power that can be drained by the passive harvester equipped with the optimal resistive load is calculated. The parameters of the model are finely tuned in Section 3 making use of experimental tests carried out with the impulsive method. The main features of the VFC are summarized in Section 4. The application of the VFC strategy to the load resistance of a cantilever harvester mounted on a car is presented in Section 5. Numerical simulations are carried out considering actual acceleration inputs measured onboard a small city car, see figure 1. Numerical results show that the VFC strategy makes it possible to double the energy storage with respect to the passive solution. Finally, conclusions are drawn in Section 6.

(**a**) (**b**)

Figure 1: SMART Fortwo of Vehicle System Dynamic and Mechatronic Lab of Sapienza: (**a**) the vehicle; (**b**) the testing equipment.

2. MODEL OF THE PIEZOELECTRIC HARVESTER

In this section, the model of a cantilever piezoelectric beam harvester, shown in figure 2, is developed as a reference to evaluate the performance of the VFC controller. This model is based on the characteristics of a PPA 1001 harvester manufactured by Midé [36], whose characteristics are listed in table 1. It is a unimorph harvester of rectangular shape and size compatible with automotive applications (41.1 x 20.8 mm). The active piezo layer is made of PZT 5H, whereas the structural layer is made of stainless steel. The piezo material satisfies the following constitutive equation [1]:

$$\begin{Bmatrix} T_1 \\ D_3 \end{Bmatrix} = \begin{bmatrix} c_{11} & -e_{31} \\ e_{31} & \varepsilon_{33} \end{bmatrix} \begin{Bmatrix} S_1 \\ E_3 \end{Bmatrix} \tag{1}$$

where D_3, E_3, T_1 and S_1 are the electric displacement, the electric field, stress, and strain, respectively and:

$$\begin{aligned} \varepsilon_{33} &= \varepsilon_{33}^{T} - d_{31}^{2} c_{11} \\ e_{31} &= d_{31} c_{11} \end{aligned} \tag{2}$$

where ε_{33}^{T} , $c_{11}$and d_{31} are the dielectric constant under constant stress, Young's modulus and the piezoelectric constant, respectively. Figure 3 shows the nomenclature of the main dimensions used for the model. Note the piezo exhibits symmetry about the $x_3 \equiv z$ axis, which is the poling axis of the material.

Table 1 General proprieties of the piezo-beam system

Material properties	**Value**
Piezo dimensions l_p x h_p x b (mm)	46 x 0.23 x 20.8
Piezo density ρ_p (kg/m^3)	7800
Piezo Young's modulus $c_{11} = 1/s_{11}^{E}$ (GPa)	60
Piezoelectric constants e_{31} $\left(\frac{C}{m^2}\right)$	-10
Permittivity constant ε_{33} $\left(\frac{nF}{m}\right)$	27.486
Beam density ρ_b (kg/m^3)	7800
Beam dimensions l_b x h_b x b (mm)	46 x 0.23 x 20.8

Young's modulus Y (GPa)	60
Integral eigenfunction $\Psi_1 = \int_0^l \phi_1(x)dx$	-0.592254
Eigenfunction derivative $\phi_1'(l)$	-984.109
Damping factor ζ_1	0.01
Natural frequency ω_1 $\left(\frac{rad}{s}\right)$	779.973

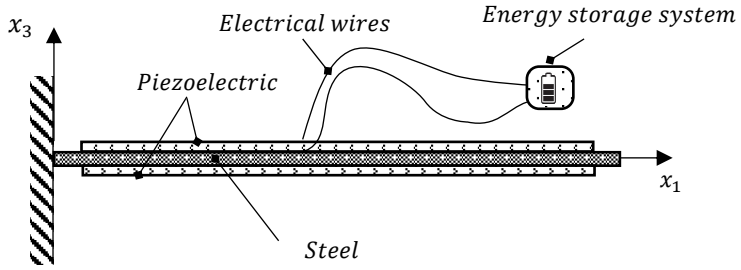

Figure 2: Clamped-free piezo-harvester.

The equation of a controlled piezo-beam system is derived from Hamilton's principle:

$$\delta J = \int_{t_1}^{t_2} (\delta T + \delta W + \delta W_{nc})\, dt = 0 \tag{3}$$

with T kinetic energy, W co-energy function and W_{nc} non-conservative energy:

$$T = \frac{1}{2}\int_0^l (\rho A \dot{w}(x,t)^2)\, dx$$
$$W = \frac{1}{2}\int_0^l dx \int_A \left(\varepsilon_{33} E_3^2 \tilde{H}(x) + 2e_{31}E_3 S_1 \tilde{H}(x) - c_{11} S_1^2 \tilde{H}(x) - Y S_1^2\right) dA \tag{4}$$

where $S_1 = -zw''$ is the strain along *x*-axes, $w(x,t)$ and $\tilde{H}(x) = H(x - l_s) - H(x - l_e)$ are the displacement along the *x*-axis and a window function with edges at the extremes of the piezo layer, respectively. l_b, l_p are the length of the beam and the length of the piezo(see figure 3). Furthermore, $\rho A = \rho_p A_p \tilde{H}(x) + \rho_b A_b$ where ρ_p, ρ_b, A_p and A_b are the piezo and beam density, and their cross-section area, respectively.

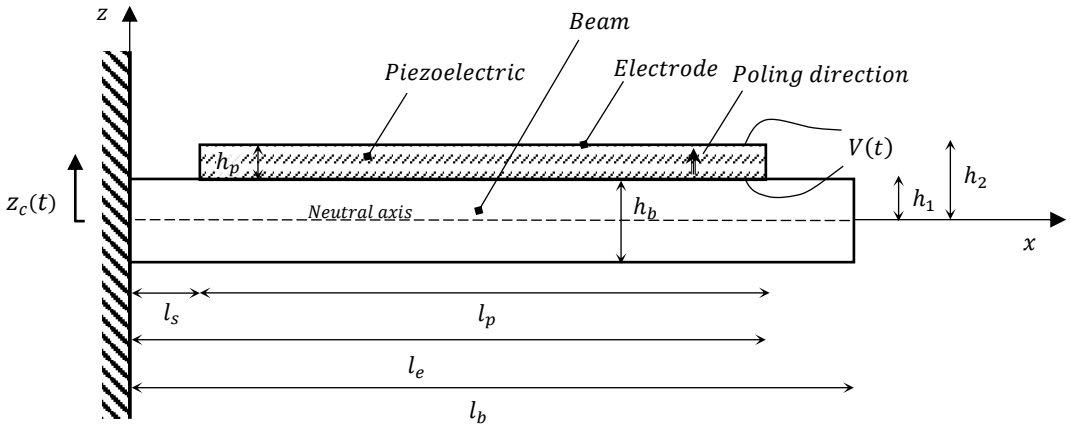

Figure 3: Main dimensions of the harvester.

The virtual work of non-conservative forces is:

$$\delta W_{nc} = \int_0^l p(x,t)\delta w \, dx - Q(t)\delta V(t) \tag{5}$$

where $p(x,t)$ and $Q(t)$ are the distributed transverse load applied to the beam and the charge over the piezo layer, respectively. $E_3 = -\frac{V(t)}{h_p}$ is the spatial uniform electrical field along the piezo, and $V(t)$ is the voltage between the electrodes. The Hamiltonian principle returns:

$$\begin{gathered}\rho A\ddot{w} + \left[-e_{31}h_m b V(t)\tilde{H}(x) + \left(c_{11}I_p\tilde{H}(x) + YI_b\right)w''\right]'' = p(x,t) \\ \frac{\varepsilon_{33}bl_p}{h_p}\dot{V}(t) + \dot{Q}(t) + e_{31}h_m b\dot{w}'\Big|_{l_s}^{l_e} = 0\end{gathered} \tag{6}$$

with boundary conditions:

$$\begin{gathered}\left[-e_{31}h_m b V(t)\tilde{H}(x) + \left(c_{11}I_p\tilde{H}(x) + YI_b\right)w''\right]\delta w'\Big|_0^l = 0 \\ \left[-e_{31}h_m b V(t)\tilde{H}(x) + \left(c_{11}I_p\tilde{H}(x) + YI_b\right)w''\right]'\delta w\Big|_0^l = 0\end{gathered}$$

where $h_m = \frac{(h_2+h_1)}{2}$, $I_p = \frac{bh_p^3}{12} + bh_p h_m^2$, $I_b = \frac{bh_b^3}{12}$, $h_p = h_2 - h_1$, $h_b = 2h_1$ and h_1, h_2 are geometrical thickness shown in figure 3, while b is the width of the piezo-beam.

The beam vertical displacement is expressed as:

$$w(x,t) = z_c(t) + w_{el}(x,t) \tag{7}$$

where $z_c(t)$ is the base vertical vibration (assumed integral with the car structure), as shown in figure 3, and $w_{el}(x,t)$ is the elastic beam vertical displacement with respect to the base. Accordingly, equations (6) become:

$$\begin{gathered}\rho A\ddot{w}_{el} + \left[\left(c_{11}I_p\tilde{H}(x) + YI_b\right)w_{el}''\right]'' = p(x,t) - \rho A\ddot{z}_c + e_{31}h_m b V(t)\tilde{H}''(x) \\ \frac{\varepsilon_{33}bl_p}{h_p}\dot{V}(t) + \dot{Q}(t) + e_{31}h_m b\dot{w}_{el}'\Big|_{l_s}^{l_e} = 0 \\ w_{el}(0,t) = w_{el}'(0,t) = 0 \\ w_{el}''(l,t) = w_{el}'''(l,t) = 0\end{gathered} \tag{8}$$

where clamped-free boundary conditions are considered.

Modal decomposition transforms equations (8) into a set of ordinary differential equations [1, 37]:

$$w_{el}(x,t) = \sum_r^\infty \phi_r(x)\eta_r(t) \tag{9}$$

$\phi_r(x)$ is the r^{th} mass-normalized eigenfunction and $\eta_r(t)$ the r^{th} modal coordinate. If ($l_p = l$) and considering the short circuit case with a generic impedance R, shown in figure 4, the equations become:

$$\begin{cases}\ddot{\eta}_r(t) + \dot{\eta}_r(t)2\zeta_r\omega_r + \eta_r(t)\omega_r^2 = \int_0^l \phi_r\left[p(x,t) - \rho(x)A\ddot{z}_c + e_{31}h_m b V(t)\tilde{H}''(x)\right] \\ C_p\dot{V}(t) + \frac{V(t)}{R} + e_{31}h_m b\sum_r^\infty \phi_r'(l)\dot{\eta}_r(t) = 0\end{cases} \text{ with } r = 1 \dots n \tag{10}$$

where $\omega_r^2 = \frac{(c_{11}I_p + YI_b)}{\rho A\, L^4}\lambda_r^4$ are the natural frequencies of the beam, λ_r the associated natural wavenumbers and $C_p = \frac{\varepsilon_{33}bl_p}{h_p}$ is the capacitance of the piezo. A proportional damping factor ζ_r is added to include dissipation inside materials and air friction is usually neglected [37, 38]. Furthermore, considering the piezoelectric is here modeled

to store energy, the derivative of the charge is posed as $\dot{Q}(t) = \frac{V(t)}{R}$, i.e. the piezo is connected to an electrical circuit with an impedance R which will be a constant value in case of a passive absorber and will be variable in the case of a semi-active absorber, as later discussed. The second of equations (10) is represented in figure 4, in which the current generator $i_{pb}(t)$ represents the vibrating mechanical coupling.

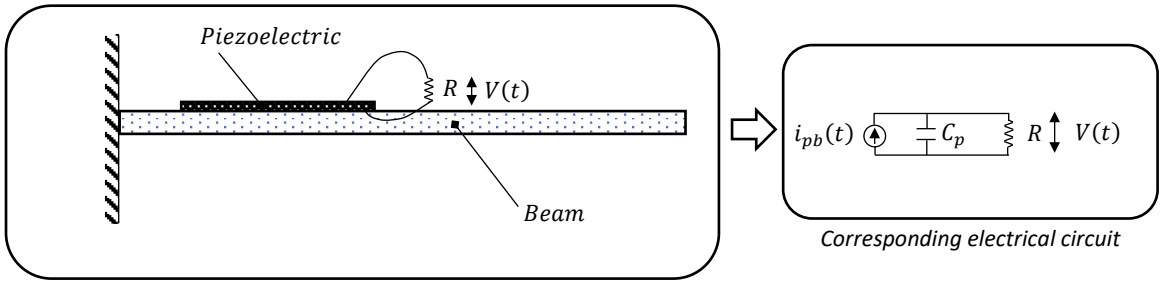

Figure 4: Clamped-free piezo-harvester and corresponding electrical circuit.

In the passive case, the optimum resistive load R must be deduced by the maximum reference power extracted by the device from the base vibrations. In this contest, the distributed transverse load applied to the beam, for example, due to the gravity force, can be neglected without losing generality. The piezoelectric voltage $V(j\omega)$ is determined from equation (10) in the Fourier domain, and the drained power can be calculated as $P(j\omega) = \frac{|V(j\omega)|^2}{R}$:

$$P(j\omega) = \frac{1}{R}\left|\left(\frac{e_{31}h_m b\sum_r^{\infty}\left(\frac{j\omega\phi_r'(l)\Psi_r\rho A}{(-\omega^2+j\omega 2\zeta_r\omega_r+\omega_r^2)}\right)}{\left((e_{31}h_m b)^2\sum_r^{\infty}\left(\frac{j\omega\phi_r'^2(l)}{(-\omega^2+j\omega 2\zeta_r\omega_r+\omega_r^2)}\right)+j\omega C_p+\frac{1}{R}\right)}\right)\right|^2 |A_c(j\omega)|^2 \qquad (11)$$

where $A_c(j\omega) = -\omega^2 Z_c$. Then the optimal value of R is the one maximizing P over a frequency band $[f_1, f_2]$.

$$P_{max} = \max_R \int_{2\pi f_1}^{2\pi f_2} P(j\omega)\, d\omega \qquad (12)$$

For a frequency band around the first resonance $[0, 300\ \text{Hz}]$ numerical maximization gives R~12kΩ.

Figure 5 shows, for several values of the resistive load, the power Frequency Response Function FRF $H_{Pow}(f)$, i.e. the ratio between the generated power $P(j\omega)$ and the second power of the base acceleration $|A_c(j\omega)|^2$, predicted by the numerical model, taking into account 3 vibration modes ($r = 3$). The resistive load has a large influence on the generated power both near the resonance and in between the resonances.

Since the resonance peaks are well separated, the study of the behavior of the harvester about the first resonance (126 Hz) can be done considering only the first mode response in the model. The results of figure 6 indicate the value $\text{R} = 12\ \text{k}\Omega$ optimizes the generated power. Figure 7 depicts the maximum power harvested P_{max} of eq. (12) in the frequency band around the first resonance $[0, 300\ \text{Hz}]$ for different values of the resistive load.

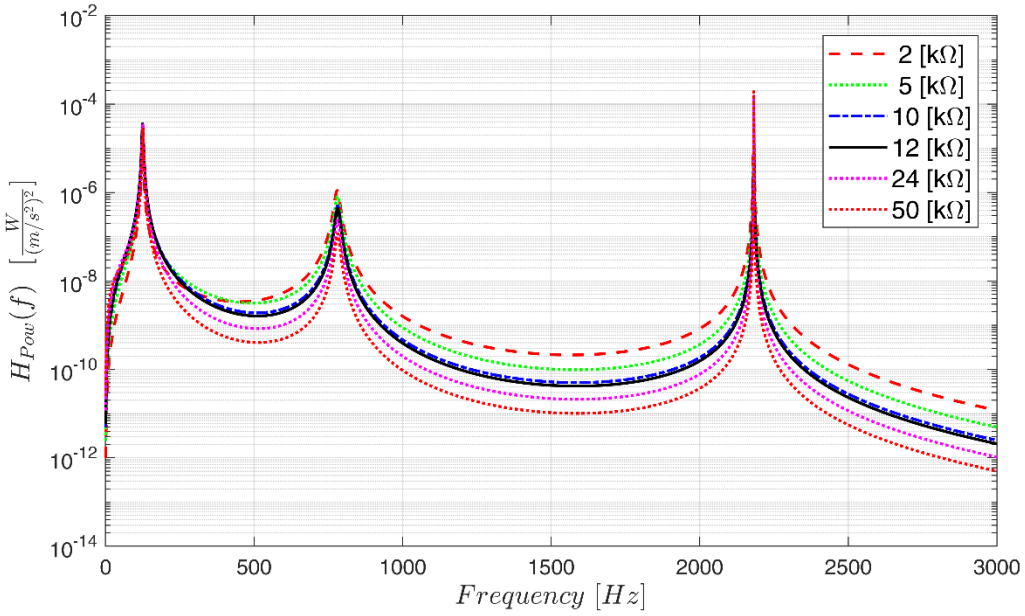

Figure 5: Power FRF of the harvester considering three modes of vibration in the model ($r = 3$).)

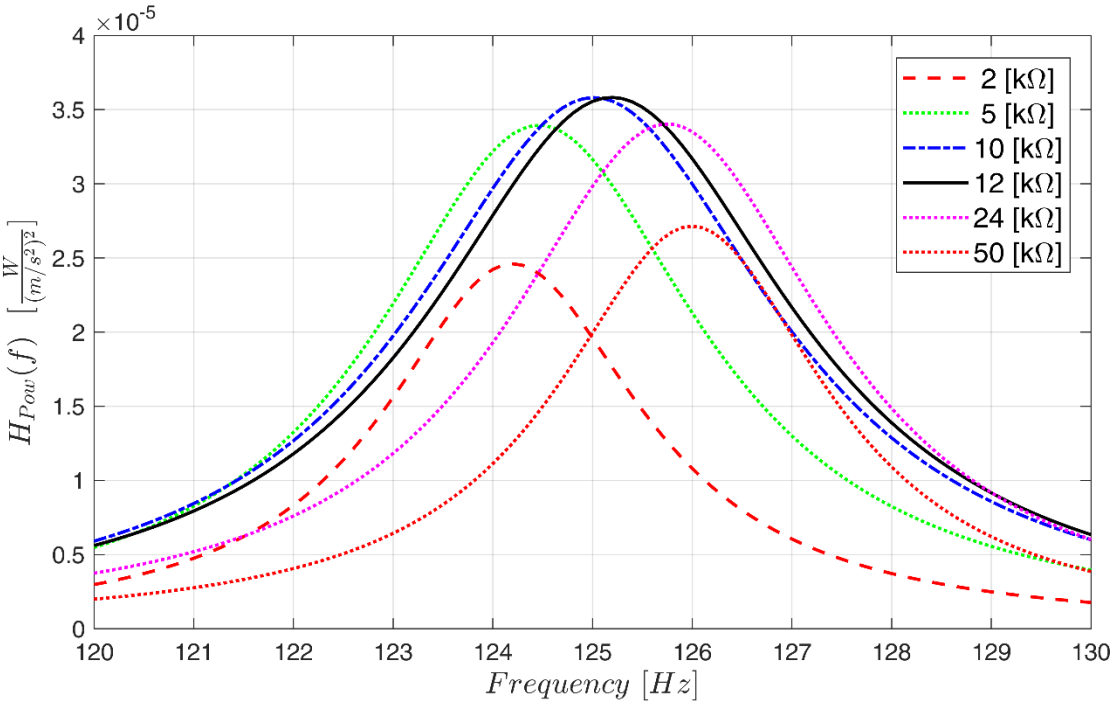

Figure 6: Energy harvester frequency response.

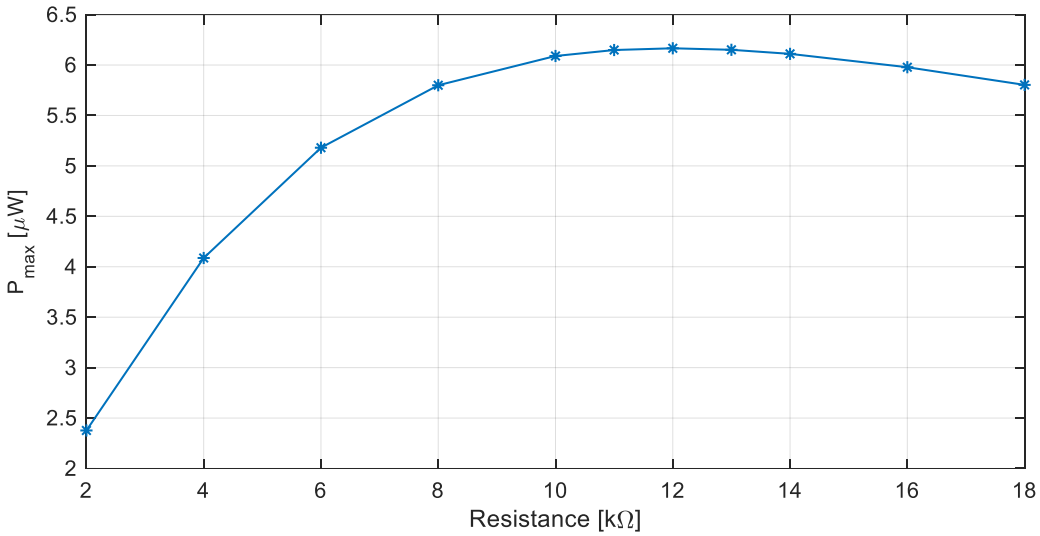

Figure 7: Maximum power harvested by varying the electrical resistance in the passive case.

3. EXPERIMENTAL TESTS

For a single-mode response, two coupled equations are derived from the eq. (10), with constant values briefly reported in table 1:

$$\begin{aligned} \ddot{\eta}_1(t) + \dot{\eta}_1(t) 2\zeta_1\omega_1 + \eta_1(t)\omega_1^2 &= -\Psi_1 \rho A \ddot{z}_c + \phi_1'(l) e_{31} h_m b V(t) \\ C_p \dot{V}(t) + \frac{V(t)}{R} + e_{31} h_m b \phi_1'(l) \dot{\eta}_1(t) &= 0 \end{aligned} \tag{13}$$

To corroborate the numerical results, the parameters of the model represented by equations (13) and (10) have been tuned for the best fitting of experimental results carried on the commercial harvester PPA-1001 [36].

Figure 8 shows the experimental setup for the measurement of the FRF between the voltage generated by the harvester and the base acceleration with the impulsive technique [39]. The harvester is clamped at one end of a stiff bar, which is excited by a hammer for modal testing at the opposite end (typically the duration of the recorded signal is 3 s and the sampling rate 4000Hz, the FRF is calculated using a fast Fourier transform). In this way, the longitudinal vibrations of the bar generated by the hammer hit excite the base of the harvester, whose vibrations are measured by a small accelerometer. The bar is suspended from a frame utilizing cables. This setup permits to decouple the resonant frequency of the piezo layer (occurring at about 120 Hz) from the very low natural frequency of the suspended bar (at about 2 Hz). The FRFs are measured for different resistive loads and each resistive load three tests are carried out.

Figure 9 displays the comparison between the experimental FRFs and the numerical FRFs calculated after the model tuning. There is an overall good agreement between experimental results and numerical simulation. Only the third experiment carried out at 24 Ω is rather different from the others with the same resistance, this result may be caused by a small fault in the wiring. Besides, it is apparent how the FRF modulus largely depends on the resistive load, with a frequency peak slightly decreasing with the decreasing of the resistive load. Eventually, Figure 10 shows the generated power as a function of the resistance value for a set of frequencies within the range $123 - 127Hz$. The the amplitude of the mono-harmonic signal is 1 g. The discussed results demonstrate how the

model represented by equations (13), with parameters given in table 1, is a good reference to simulate the behavior of the typical piezo energy harvester.

In the following sections, this model is combined with a self-adapting resistor $R(t)$ made time-dependent through the use of a standard circuitry. In particular, the resistance value is controlled as a function of the voltage at the piezoelectrical terminals, which is obeying the control law recently introduced by the authors for semi-active mechanical suspension devices [28].

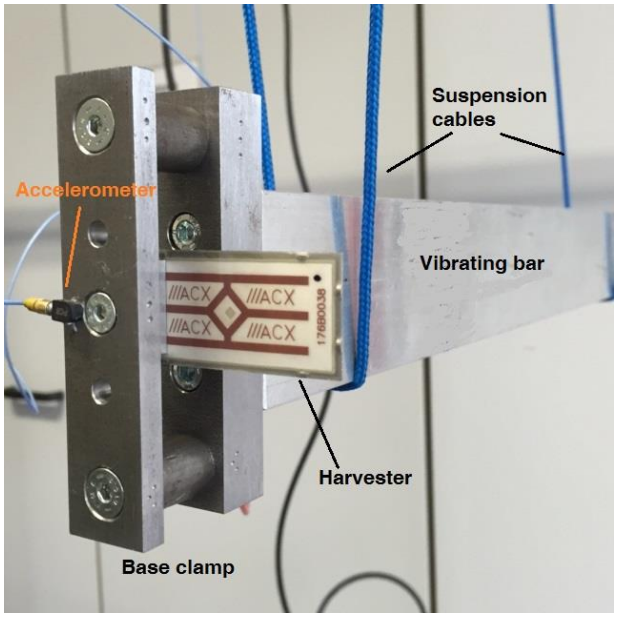

Figure 8: Testing equipment with the suspended vibrating bar, the harvester and the accelerometer.

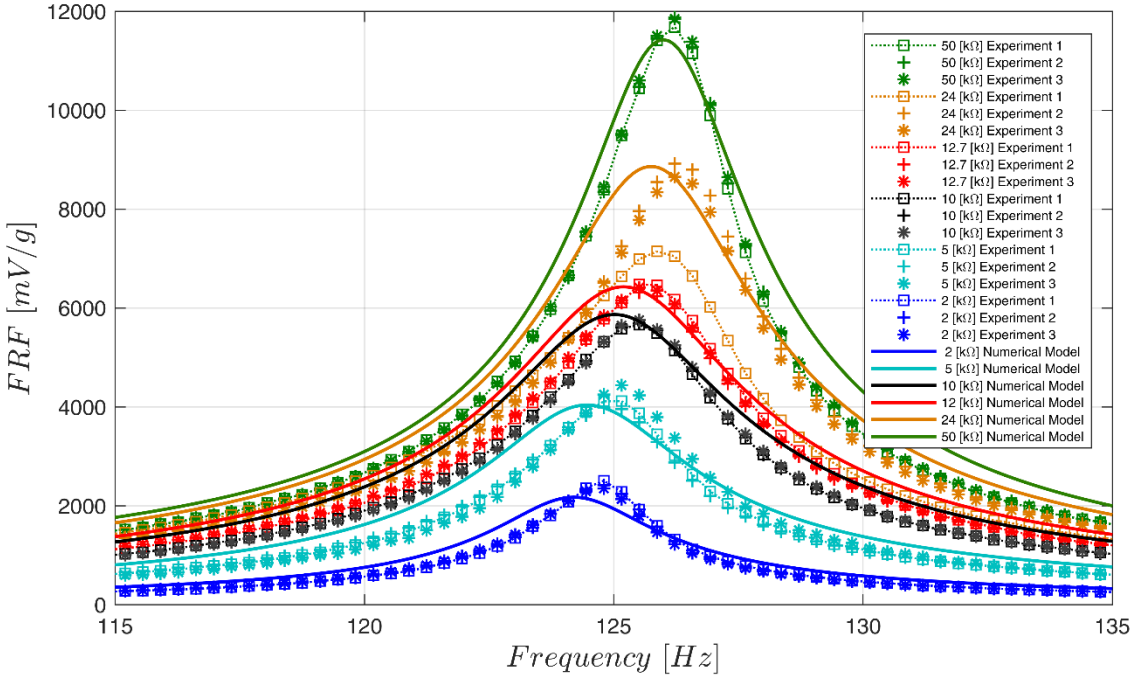

Figure 9: Numerical VS Experimental FRF of PPA 1001 with different resistive loads.

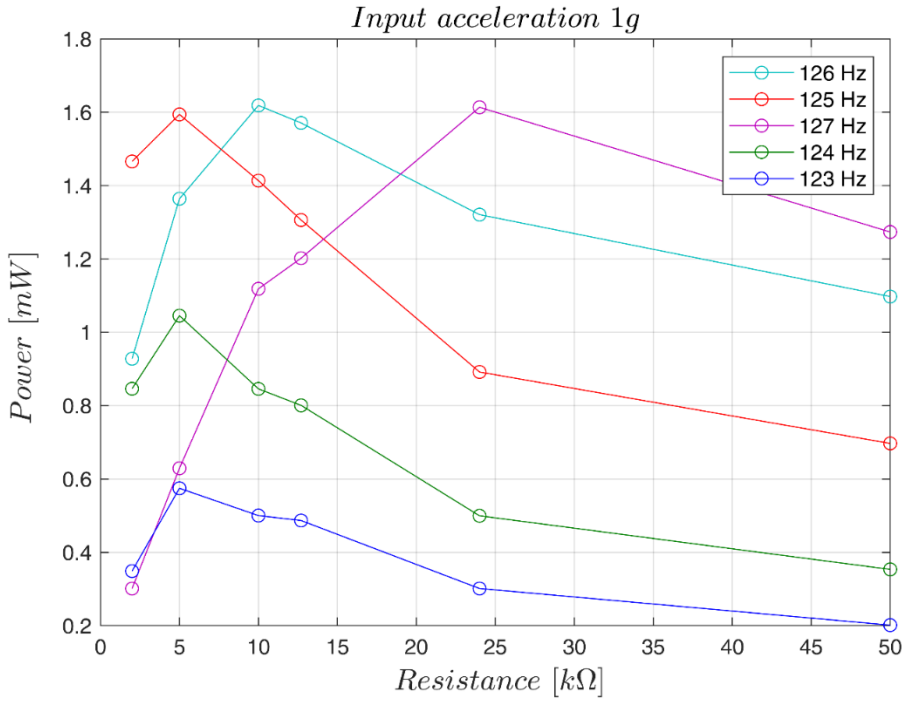

Figure 10: effect of load resistance on experimental powers at assigned frequencies.

4. HARVESTER BOOSTING BY SEMI-ACTIVE CONTROL

In this section, the boosting strategy for semi-active control of the harvester is introduced and it is based on the Variational Feedback Control (VFC) [28, 31, 40-43], whose description is briefly reported.

The VFC is derived from the variational principle based on Pontryagin's method [28, 44]. In general, such procedure aims to minimize a cost function J in time domain, which is equal to the integral of an objective function L depending on the state $\boldsymbol{x}(t)$, the control $\boldsymbol{u}(t)$ and an external disturbance $\boldsymbol{y}(t)$:

$$\begin{cases} J = \int_{t_0}^{t_f} L(\boldsymbol{x}(t), \boldsymbol{u}(t), \boldsymbol{y}(t))dt \quad : \quad \underset{\boldsymbol{u}\in U}{Opt}\, J \\ \dot{\boldsymbol{x}}(t) = \boldsymbol{f}(\boldsymbol{x}(t), \boldsymbol{u}(t), \boldsymbol{y}(t)) \\ \boldsymbol{x}(t_0) = \boldsymbol{x}_{t_0} \end{cases} \tag{14}$$

where $\dot{\boldsymbol{x}} = \boldsymbol{f}(\boldsymbol{x}, \boldsymbol{u}, \boldsymbol{y})$ is the dynamic equation of the controlled dynamical system with initial condition $\boldsymbol{x}(t_0) = \boldsymbol{x}_{t_0}$ and $\boldsymbol{u} \in U$ represents the restraints for the control variable, related to the technical limitations of the employed actuators. The variational calculus permits to maximize/minimize J. The method of Lagrangian multipliers $\boldsymbol{\lambda}$ is used, leading to the following formulation:

$$\begin{cases} \delta\tilde{J} = \delta \int_{t_0}^{t_f} L(\boldsymbol{f}(\boldsymbol{x}, \boldsymbol{u}, \boldsymbol{y}), \boldsymbol{y}) + \boldsymbol{\lambda}^T\big(\dot{\boldsymbol{x}} - \boldsymbol{f}(\boldsymbol{x}, \boldsymbol{u}, \boldsymbol{y})\big)dt \; = 0 \\ \boldsymbol{x}(t_0) = \boldsymbol{x}_{t_0} \end{cases} \tag{15}$$

By operating the functional variations, the following Euler-Lagrange equations, and the associated transversality conditions are produced:

$$\begin{cases} \big(L_{\boldsymbol{f}} - \boldsymbol{\lambda}\big)^{\boldsymbol{T}} \boldsymbol{f}_{\boldsymbol{x}} = \; \dot{\boldsymbol{\lambda}}^T \\ \big(L_{\boldsymbol{f}} - \boldsymbol{\lambda}\big)^{\boldsymbol{T}} \boldsymbol{f}_{\boldsymbol{u}} = \boldsymbol{0}^T \\ \dot{\boldsymbol{x}} = \boldsymbol{f}(\boldsymbol{x}, \boldsymbol{u}, \boldsymbol{y}) \\ \boldsymbol{x}(t_0) = \boldsymbol{x}_{t_0} \\ \boldsymbol{\lambda}^{\boldsymbol{T}}(t_f)\delta\boldsymbol{x}(t_f) = 0 \end{cases} \tag{16}$$

where $\boldsymbol{f}_{\boldsymbol{x}} = \frac{\partial f_i}{\partial x_j}$ and $\boldsymbol{f}_{\boldsymbol{u}} = \frac{\partial f_i}{\partial u_j}$ are the Jacobian matrixes. The VFC restricts the family to which L and $\boldsymbol{f}$ belong. In the present analysis, it is assumed:

$$L(\boldsymbol{f}, \boldsymbol{y}) = \boldsymbol{f}^T\boldsymbol{Q}\boldsymbol{f} + \boldsymbol{f}^T\boldsymbol{T}\boldsymbol{y} = \dot{\boldsymbol{x}}^T\boldsymbol{Q}\dot{\boldsymbol{x}} + \dot{\boldsymbol{x}}^T\boldsymbol{T}\boldsymbol{y} \tag{17}$$

where $\boldsymbol{Q}$ e $\boldsymbol{T}$ are gain matrices, whose coefficients are tuned to optimize the control law. Expression (17) represents a generalized state-rate $\dot{\boldsymbol{x}}$ quadratic form and it is completed by a bilinear form in terms of the state and the external action $\boldsymbol{y}$. The VFC control give the chance to solve the Pontryagin problem in the feedback way thanks to the special form of the objective function where L takes the quadratic form of the dynamic equation minimization and its product over the disturbances. This means that the control solution will minimize the entire state vector $\dot{\boldsymbol{x}}$ as well as the power entering the electromechanical system. External disturbances that excite the system will be converted into energy to be stored. Furthermore, also a quadratic form in terms of the state $\boldsymbol{x}$ can be included by using the augmented state $\boldsymbol{q} = [\boldsymbol{x}, \boldsymbol{I}]^{\boldsymbol{T}}, \dot{\boldsymbol{I}} = \; \boldsymbol{x}$ with dynamic equation $\dot{\boldsymbol{q}} = \boldsymbol{g}(\boldsymbol{q}, \boldsymbol{u}) = [\boldsymbol{f}, \boldsymbol{x}]^T$, that produces the new objective function:

$$L'(\boldsymbol{g}, \boldsymbol{y}) = \boldsymbol{q}^T\boldsymbol{Q}'\boldsymbol{q} + \boldsymbol{q}^T\boldsymbol{T}'\boldsymbol{y} \tag{18}$$

The equation of motion is of an affine-control type:

$$\boldsymbol{f}(\boldsymbol{x},\boldsymbol{u},\boldsymbol{y}) = \boldsymbol{\varphi}(\boldsymbol{x},\boldsymbol{y}) + \boldsymbol{S}(\boldsymbol{x},\boldsymbol{y})\boldsymbol{u} \tag{19}$$

i.e. it is nonlinear in the state, but linear in the control. It is shown in [28] that the optimal solution $\boldsymbol{u}^*$ of the previous problem, defined by the functional (17) with the differential constraint (19), is set in the form:

$$\boldsymbol{u}^* = \left[\widetilde{\boldsymbol{Q}}\boldsymbol{S}(\boldsymbol{x},\boldsymbol{y})\right]^+\left[-\widetilde{\boldsymbol{Q}}\boldsymbol{\varphi}(\boldsymbol{x},\boldsymbol{y}) - \mathbf{T}\boldsymbol{y}\right] \tag{20}$$

where $\widetilde{\boldsymbol{Q}} = \boldsymbol{Q} + \boldsymbol{Q}^T$, and the symbol "+" indicates pseudo-inverse. To account for the control saturation $\boldsymbol{u} \in \boldsymbol{U}$, the control variable constraint is managed as follows:

$$\begin{cases} \boldsymbol{u}^* \in U \rightarrow \ \boldsymbol{u} = \boldsymbol{u}^* \\ \boldsymbol{u}^* \notin U \rightarrow \ \boldsymbol{u} = \boldsymbol{u}_{\partial U} \end{cases} \tag{21}$$

generally known as the clipping technique where $\boldsymbol{u}_{\partial U}$ are the control values at the frontier of the space U.

5. HARVESTER PERFORMANCE ESTIMATION: COUPLING EXPERIMENTAL DATA AND NUMERICAL SIMULATIONS

The state-space model associated with equation (13) according to (19) is:

$$\dot{\boldsymbol{x}} = \boldsymbol{\varphi}(\boldsymbol{x},\boldsymbol{y}) + \boldsymbol{S}(\boldsymbol{x})u \tag{22}$$

where:

$$\boldsymbol{\varphi}(\boldsymbol{x},\boldsymbol{y}) = \begin{bmatrix} 0 & 1 & 0 \\ -\omega_1^2 & -2\zeta_1\omega_1 & \phi_1'(l)e_{31}h_m b \\ 0 & -\dfrac{e_{31}h_m b}{C_p}\phi_1'(l) & 0 \end{bmatrix}\begin{bmatrix}\eta \\ \dot{\eta} \\ V\end{bmatrix} + \begin{bmatrix} 0 \\ -\Psi_r\rho A\ddot{z}_c \\ 0 \end{bmatrix} \quad ; \quad \boldsymbol{S}(\boldsymbol{x}) = \begin{bmatrix} 0 \\ 0 \\ -\dfrac{V}{C_p} \end{bmatrix} \tag{23}$$

$$\boldsymbol{x} = \begin{bmatrix}\eta \\ \dot{\eta} \\ V\end{bmatrix} \quad ; \quad u = \frac{1}{R} \quad ; \quad \boldsymbol{y} = \begin{bmatrix} 0 \\ -\Psi_r\rho A\ddot{z}_c \\ 0 \end{bmatrix}$$

Using the explicit control solution (20), described in the previous section, equation (23) produces:

$$u^* = \frac{1}{R^*} = \frac{g_1 * \eta + g_2 * \dot{\eta} + g_3 * V + g_4 * \ddot{z}_c}{V} \tag{24}$$

that represents the optimal control law to maximize the performance of the harvester. The g_i constants are unknown tuning parameters that arise from a nonlinear combination of $\boldsymbol{Q}$ and $\boldsymbol{T}$ coefficients of equation (18).

The equivalent circuit of the optimally controlled piezo harvester is shown in figure 11, where the control parameter is $u^* = \frac{1}{R^*}$, i.e. a variable resistive load. This device is technically implementable using an operational amplifier circuitry and it can control the electrical impedance at any time.

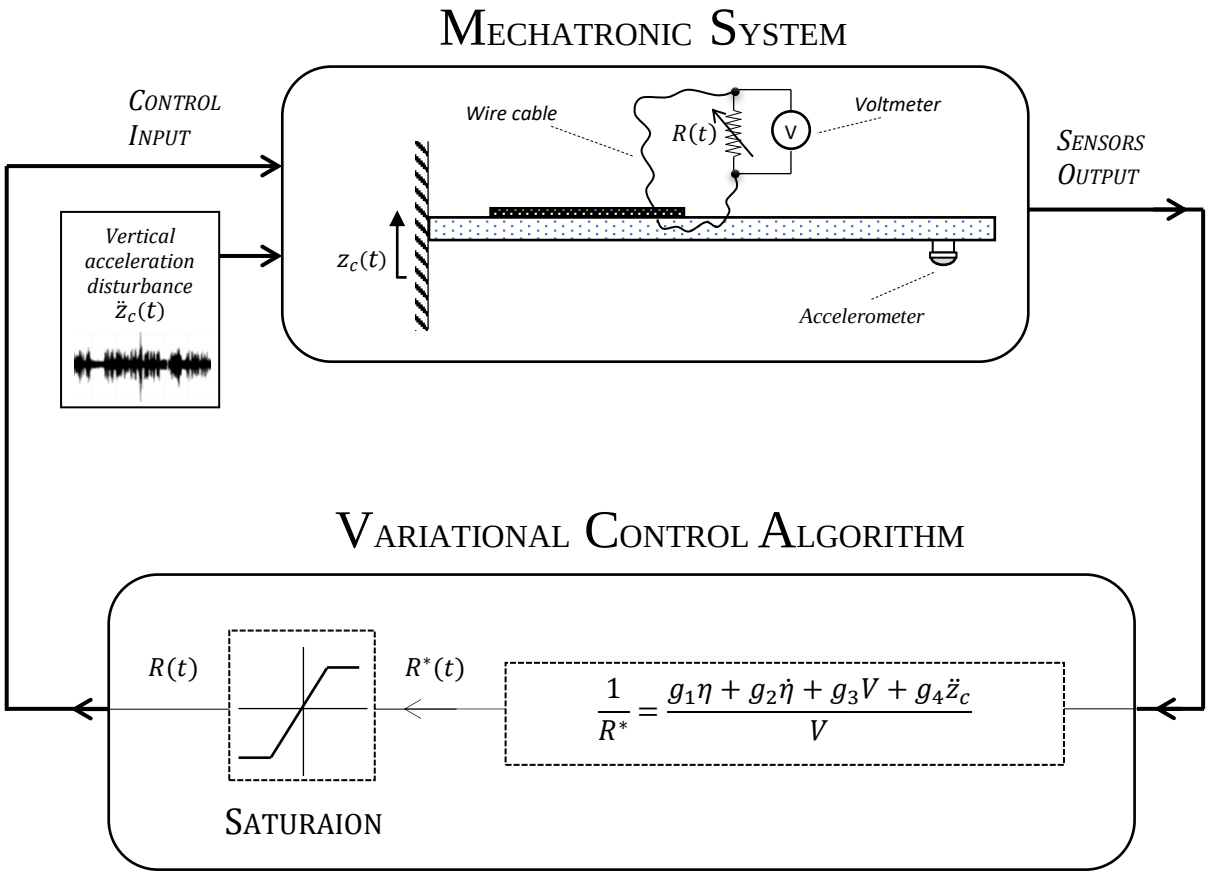

Figure 11: VFC control diagram of the mechatronic system energy accumulator

The resistance value $R(t)$ is saturated by a simple clipping procedure as shown in the control diagram shown in figure 11:

$$\begin{cases} R = R_{max} & if \quad R^* \geq R_{max} \\ R = R_{min} & if \quad R^* < R_{min} \end{cases} \tag{25}$$

The simulations are carried out considering acceleration values experimentally measured onboard one of the instrumented cars of the Vehicle System Dynamic and Mechatronic Lab of Sapienza. Figures 12 shows the experimental setup used to acquire the vertical vibration of the moving vehicle. The piezoelectric accelerometer, installed on the chassis near the main excitation point, i.e. the engine compartment, is acquired for almost one hour of an extra-urban cycle. The accelerometer used has high sensitivity, 100mV/g, and a max frequency band up to 10kHz. In figure 13, a time record with a 20kHz sample frequency of the measured acceleration is reported and in figure 14 a zoom of the power spectral density, to highlight the greatest oscillations occurs at low-frequency band [0-500]Hz is shown.

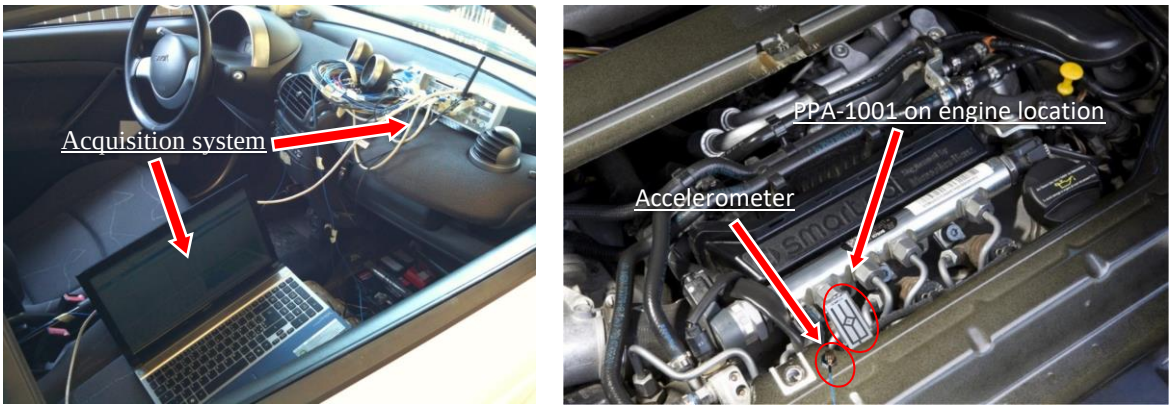

(a) (b)

Figure 12: Setup of the acquisition system (a); Piezo PPA-1001 on Smart Fortwo engine chassis with piezo accelerometer (b).

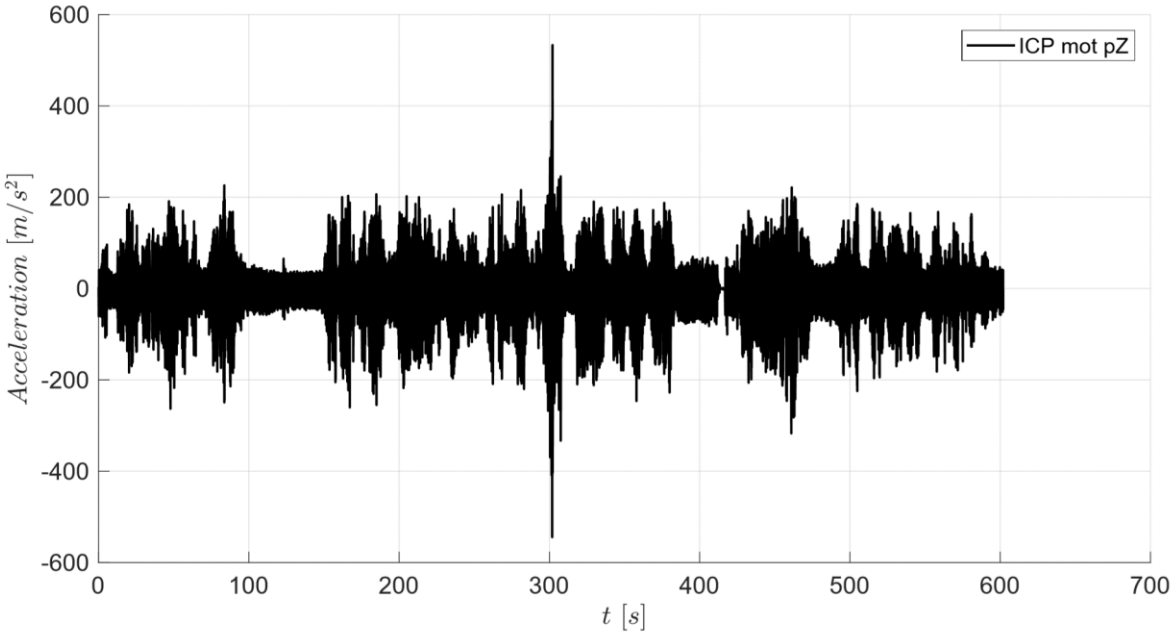

Figure 13: Motor chassis acceleration of an extra-urban cycle

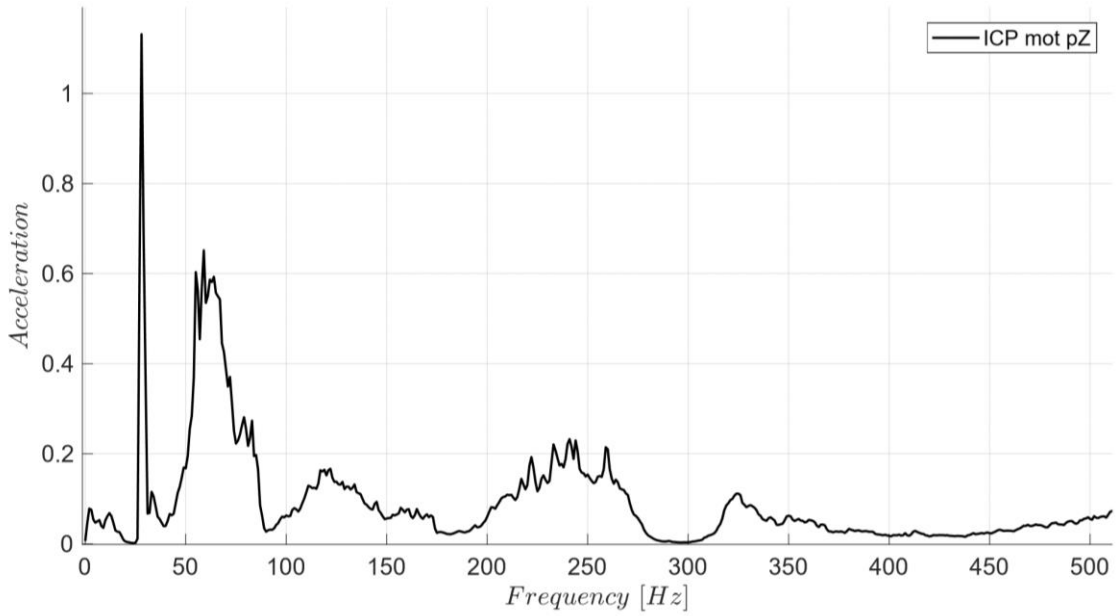

Figure 14: Power spectral density (PSD) of motor chassis acceleration of an extra-urban cycle $\left[\left(\frac{m}{s^2}\right)^2/Hz\right]$

Equation (24) represents the final form of the VFC used to maximize the electrical energy to be accumulated through the variation of resistance R. The gain parameters g_i are identified through the aid of an evolutionary algorithm called Genetic Algorithm (GA), i.e. a parametric optimization algorithm inspired by the Darwinian natural evolution [45]. The genetic algorithm has the objective function of determining the optimal combination of the g_i unknown parameters for which the average accumulated energy is the highest possible. This was performed by imposing two types of control, a fast called *VFC case 1* and a slow control *VFC case 2*, both supposing a single-mode response, numerically solving the equation (13). In the case of fast control, the simulation of the electromechanical model was performed by saturating the control frequency up to 5kHz while in the case of slow control the saturation reaches 1kHz. The slow saturation is applied through the use of a first-order differential equation that simulates the delay time in the control response. The Table 2 shows the g_i values found by the GA and the result of the objective function, that is the mean harvested energy. The numerical results are shown in figures 15 and 16 and both are compared with the dynamic behavior in the case of passive control, i.e. by choosing a constant resistance equal to $\mathrm{R} = 12\ \mathrm{k\Omega}$ because, as confirmed by Figure 7, it corresponds to the maximum accumulable electrical power.

The GA optimal setting for case 1 is reported in table 2 where only g_2 has a non-zero value. The associated power (see figure 15) shows a sequence of periodic large peaks, which are the distinctive elements of the VFC semi-active control. The instant power at the peaks reaches the level of few milliwatts. This control effect guarantees the average storage of energy of about two times the one stored with the optimized passive resistive load (see Table 2 that refers to a test duration of 1 hour). The control logic suggests a maximum saturation of the resistance higher than the passive one, reaching about $R_{max} = 400\ \mathrm{k\Omega}$ and a lower value R_{min} that does not drop below zero. The type of control shows a high level of intermittency and indicates the technical realization of the circuitry does not need any continuously variable resistor, but a simpler on-off switch piloted by a transistor to load and unload a parallel resistor on the piezoelectric (see figure 17(a)). However, the intermittency requires that the energy

storage management system is made up of fast capacitors to quickly collect the current circulating within the electrical circuit.

The second control strategy, VFC case 2, uses only the optimal setting of the gain g_1. Once again, energy storage close to being twice the one obtained by the purely passive circuit is achieved, see table 2. The advantage of this type of tuning relies on a much smoother control action, in fact, unlike the previous strategy, it will require much slower electronics to manage and store energy with no need for fast capacitors. On a contrary a more sophisticated control circuit to manage a variable resistor is required that can be implemented via operational amplifiers as sketched in figure 17(b). In both cases, higher accumulated energies are achieved concerning the passive case, confirming improved performances.

Moreover, it is important to note that the total energy stored must necessarily be subtracted from the energy spent to perform the measure and the power supply of the controller. On the electronic market, micro accelerometers, as well as strain gauge sensors, can be found with low consumption, around μW, as referred in [46-48]. In addition to the use of sensors, a low consumption microcontroller is required to control the resistance of the electrical circuit and apply the control law thanks to an analog-digital converter. Inside the microcontroller, it will be possible to implement a state observer, for example, an extended Kalman filter or other methods [49, 50], to correctly estimate the variables necessary for the application of the control law. In the automotive application, the amplitude of accelerations due to engine vibrations mostly excites low frequencies in the range of [0-300] Hz, as shown in figure 14, a bandwidth that includes the first piezoelectric cantilever mode at almost 125Hz, easily appreciable from a state observer.

Table 2 Comparison of energy harvesting, extra-urban cycle, duration 1 hours

Control parameters	**Mean harvested energy** $[mJ]$
Passive	46.8
VFC case1: $g_2 = 90;\ g_1 = g_3 = g_4 \approx 0$	93.6
VFC case2: $g_1 = -60;\ g_2 = g_3 = g_4 \approx 0$	72

As an example, $93.6mJ \times 200 = 18.7J$ can be harvested, considering one hour of VFC case1 of energy harvesting and 200 piezo-beam pieces, of about 0.6kg overall weight on board of a SMART car, located in the engine compartment (see figure 12(b)). The order of magnitude of the expected power is $\frac{18.7J}{3600s} = 5mW$ and the specific power is about $3mW/kg$ where the weight of the electronic board and sensors is roughly supposed 0.8Kg for all 200 pieces. The electronic board, from an electrical engineering point of view, should read data sensors, vary the resistors and converting the alternating voltage output via operational circuits.

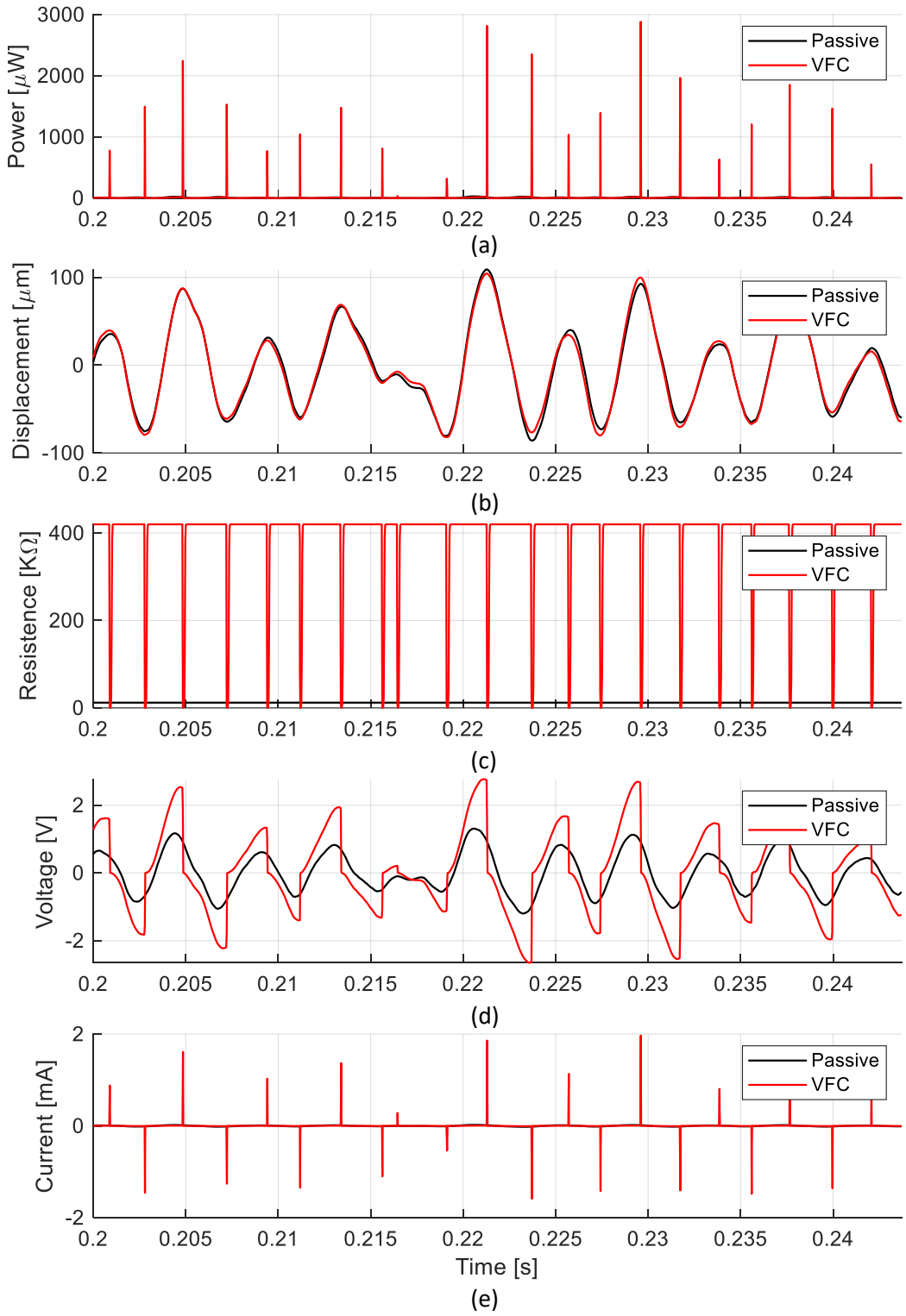

Figure 15: Power storage (a), tip beam displacement (b), resistance (c), voltage (d) and current (e) of VFC case 1 vs Passive control (from top to bottom)

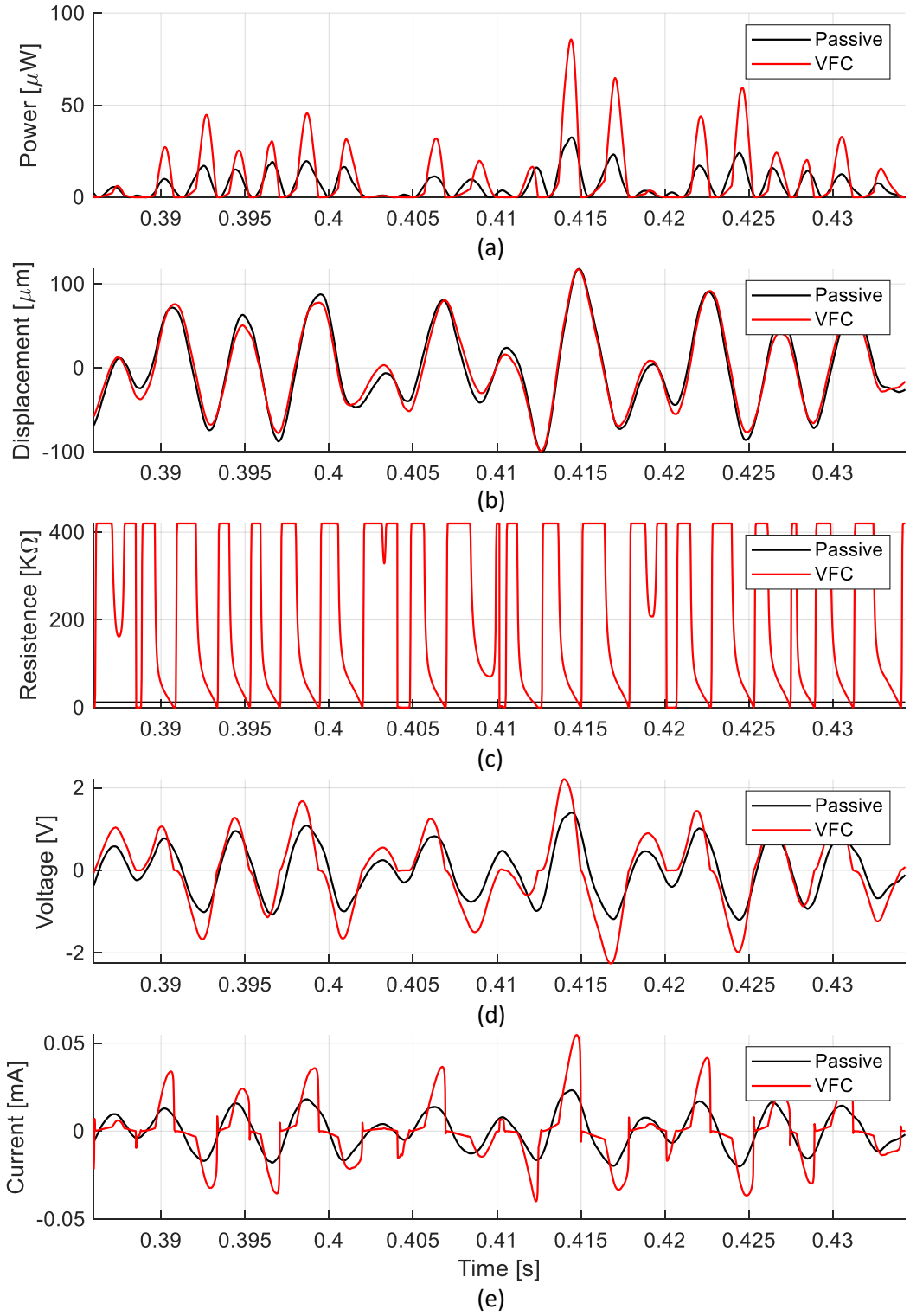

Figure 16: Power storage (a), tip beam displacement (b), resistance (c), voltage (d) and current (e) of VFC case 2 vs Passive control (from top to bottom)

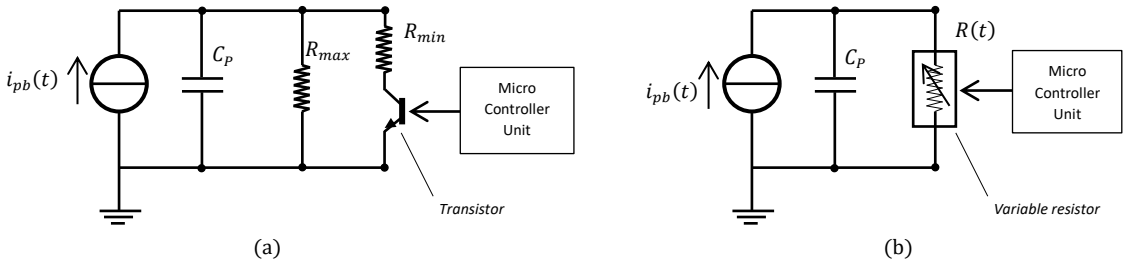

Figure 17: Circuit diagram with switch transistor (a) and variable resistance (b).

6. CONCLUSION

This paper investigates the upper bound of the energy that can be harvested by piezoelectric devices installed on the board of cars. To this aim, a commercial harvester has been selected, experimentally tested, and a harvester model has been developed and tuned by means of experimental results. Moreover, a small urban car has been tested to acquire the vibration spectra at different locations, where it is meaningful to install the energy harvesters. The performance of the commercial harvester is boosted by using an adaptive impedance control of its resistive part. This operation is obtained by applying a novel control method recently proposed by the authors, the Variational Feedback Control law (VFC). Classical methods of passive energy harvesting are often based on resonance effects, but the high sensitivity of the output power to the external frequency excitation induces poor performances in presence of a wide spectrum excitation. Semi-active energy harvesters are generally based on empirical control law; instead, in this paper, VFC introduces a rationale for a smart adaptive mechanism with the explicit and strict target of maximizing the output power. The vibrations coming from the rough road, crossing bumps, road holes, and the internal combustion engine become suitable sources of energy that can be converted into electrical energy through an array of vibrating piezo harvesters, driven by a suitable microcontroller. With lightweight instrumentation and the mass of 200 piezo-beam pieces, it is possible to obtain, using the semi-adaptive impedance method presented in this paper, a power output of about $5mW$, with an order of magnitude of the power density upper bound of about $3mW/kg$.

It appears that from an energy point of view, the power produced due to the car vibrations does not exhibit any possible advantage in terms of energy saving. A car of the type here considered shows a power to mass ratio of about $20W/kg$. Comparing this value with the one obtained as power recovery, $3mW/kg$, implies that, on average, the cost of transport of the harvester weight harvester is 6600 times the savings the harvester allows. However, in some cases, the harvester can allow some constructive simplifications related to the local availability of the power, for example, to supply vehicle bulbs or vehicle instrumentations, eliminating the manufacturing costs of wired power supply.

REFERENCES

[1] S. Priya and D. J. Inman, *Energy Harvesting Technologies*. Springer US, 2008.

[2] B. Kaltenbacher and P. Krejčí, "Analysis of an optimization problem for a piezoelectric energy harvester," *Archive of Applied Mechanics*, Article vol. 89, no. 6, pp. 1103-1122, 2019, doi: 10.1007/s00419-018-1459-6.

[3] A. Erturk and D. Inman, *An Experimentally Validated Bimorph Cantilever Model for Piezoelectric Energy Harvesting from Cantilevered Beams*. 2009, pp. 25009-18.
[4] Y. C. Shu and I. C Lien, *Analysis of power output for piezoelectric energy harvesting systems*. 2006, p. 1499.
[5] J. Dicken, P. D. Mitcheson, I. Stoianov, and E. M. Yeatman, "Power-Extraction Circuits for Piezoelectric Energy Harvesters in Miniature and Low-Power Applications," *IEEE Transactions on Power Electronics*, vol. 27, no. 11, pp. 4514-4529, 2012, doi: 10.1109/TPEL.2012.2192291.
[6] R. D. hulst and J. Driesen, "Power processing circuits for vibration-based energy harvesters," in *2008 IEEE Power Electronics Specialists Conference*, 15-19 June 2008 2008, pp. 2556-2562, doi: 10.1109/PESC.2008.4592325.
[7] Y. C. Shu, I. C. Lien, and W. J. Wu, "An improved analysis of the SSHI interface in piezoelectric energy harvesting," *Smart Materials and Structures*, vol. 16, no. 6, p. 2253, 2007.
[8] V. Cossalter, A. Doria, S. Garbin, and R. Lot, "Frequency-domain method for evaluating the ride comfort of a motorcycle," *Vehicle System Dynamics*, vol. 44, no. 4, pp. 339-355, 2006/04/01 2006, doi: 10.1080/00423110500420712.
[9] F. Orfei, H. Vocca, and L. Gammaitoni, "Linear and Non Linear Energy Harvesting From Bridge Vibrations," no. 50206, p. V008T10A054, 2016, doi: 10.1115/DETC2016-59650.
[10] M. Zhou and H. Zhao, "Revisit to the theoretical analysis of a classical piezoelectric vibration energy harvester," *Archive of Applied Mechanics*, Article vol. 90, no. 11, pp. 2379-2395, 2020, doi: 10.1007/s00419-020-01727-x.
[11] T. J. Kaźmierski and S. Beeby, *Energy Harvesting Systems: Principles, Modeling and Applications* (SpringerLink : Bücher). Springer New York, 2010.
[12] M. Nazemizadeh, F. Bakhtiari-Nejad, A. Assadi, and B. Shahriari, "Size-dependent nonlinear dynamic modeling and vibration analysis of piezo-laminated nanomechanical resonators using perturbation method," *Archive of Applied Mechanics*, Article vol. 90, no. 8, pp. 1659-1672, 2020, doi: 10.1007/s00419-020-01678-3.
[13] A. Paknejad, G. Rahimi, and H. Salmani, "Analytical solution and numerical validation of piezoelectric energy harvester patch for various thin multilayer composite plates," *Archive of Applied Mechanics*, Article vol. 88, no. 7, pp. 1139-1161, 2018, doi: 10.1007/s00419-018-1363-0.
[14] A. Doria, C. Medè, G. Fanti, D. Desideri, A. Maschio, and F. Moro, *Development of Piezoelectric Harvesters with Integrated Trimming Devices*. 2018, p. 557.
[15] S. Dhote, Z. Yang, and J. Zu, "Modeling and experimental parametric study of a tri-leg compliant orthoplanar spring based multi-mode piezoelectric energy harvester," *Mechanical Systems and Signal Processing*, 21_Publication in refereed journal vol. 98, pp. 268-280, 1/1 2018, doi: 10.1016/j.ymssp.2017.04.031.
[16] N. V. Viet, W. Zaki, and R. Umer, "Analytical investigation of an energy harvesting shape memory alloy–piezoelectric beam," *Archive of Applied Mechanics*, Article vol. 90, no. 12, pp. 2715-2738, 2020, doi: 10.1007/s00419-020-01745-9.
[17] S. Mojrzisch and J. Twiefel, "Phase-controlled frequency response measurement of a piezoelectric ring at high vibration amplitude," *Archive of Applied Mechanics*, Article vol. 86, no. 10, pp. 1763-1769, 2016, doi: 10.1007/s00419-015-1032-5.
[18] R. Ramlan, M. J. Brennan, B. R. Mace, and S. G. Burrow, "On the performance of a dual-mode non-linear vibration energy harvesting device," *Journal of Intelligent Material Systems and Structures*, vol. 23, no. 13, pp. 1423-1432, 2012/09/01 2012, doi: 10.1177/1045389X12443017.
[19] D. Castagnetti and E. Radi, "A piezoelectric based energy harvester with dynamic magnification: modelling, design and experimental assessment," *Meccanica*, Article vol. 53, no. 11-12, pp. 2725-2742, 2018, doi: 10.1007/s11012-018-0860-0.
[20] G. De Pasquale, "Artificial human joint for the characterization of piezoelectric transducers in self-powered telemedicine applications," *Meccanica*, Article vol. 51, no. 9, pp. 2259-2275, 2016, doi: 10.1007/s11012-016-0359-5.
[21] A. Syta, C. R. Bowen, H. A. Kim, A. Rysak, and G. Litak, "Experimental analysis of the dynamical response of energy harvesting devices based on bistable laminated plates," *Meccanica*, Article vol. 50, no. 8, pp. 1961-1970, 2015, doi: 10.1007/s11012-015-0140-1.
[22] G. Xia, F. Fang, Q. Wang, M. Zhang, and J. Wang, "Performance analysis of piezoelectric energy harvesters with a tip mass and nonlinearities of geometry and damping under parametric and external excitations," *Archive of Applied Mechanics*, Article 2020, doi: 10.1007/s00419-020-01721-3.
[23] G. Xia, F. Fang, M. Zhang, Q. Wang, and J. Wang, "Performance analysis of parametrically and directly excited nonlinear piezoelectric energy harvester," *Archive of Applied Mechanics*, Article vol. 89, no. 10, pp. 2147-2166, 2019, doi: 10.1007/s00419-019-01568-3.
[24] G. K. Ottman, H. F. Hofmann, A. C. Bhatt, and G. A. Lesieutre, "Adaptive piezoelectric energy harvesting circuit for wireless remote power supply," *IEEE Transactions on Power Electronics*, vol. 17, no. 5, pp. 669-676, 2002, doi: 10.1109/TPEL.2002.802194.

[25] D. Guyomar and M. Lallart, "Recent Progress in Piezoelectric Conversion and Energy Harvesting Using Nonlinear Electronic Interfaces and Issues in Small Scale Implementation," *Micromachines*, vol. 2, no. 2, 2011, doi: 10.3390/mi2020274.

[26] Lefeuvre E., Badel A., Brenes A., Seok S., Woytasik M., and Yoo C. S., "Analysis of piezoelectric energy harvesting system with tunable SECE interface," *Smart Materials and Structures*, vol. 26, no. 3, p. 035065, 2017.

[27] K. B. Singh, V. Bedekar, S. Taheri, and S. Priya, "Piezoelectric vibration energy harvesting system with an adaptive frequency tuning mechanism for intelligent tires," *Mechatronics*, vol. 22, no. 7, pp. 970-988, 2012/10/01/ 2012, doi: https://doi.org/10.1016/j.mechatronics.2012.06.006.

[28] G. Pepe and A. Carcaterra, "VFC – Variational Feedback Controller and its application to semi-active suspensions," *Mechanical Systems and Signal Processing*, 2016, doi: http://dx.doi.org/10.1016/j.ymssp.2016.01.002.

[29] G. Pepe, N. Roveri, and A. Carcaterra, "Prototyping a new car semi-active suspension by variational feedback controller," in *Proceedings of ISMA 2016 - International Conference on Noise and Vibration Engineering and USD2016 - International Conference on Uncertainty in Structural Dynamics*, 2016, pp. 231-245. [Online]. Available: https://www.scopus.com/inward/record.uri?eid=2-s2.0-85018191875&partnerID=40&md5=e88d23db689766f93f188de213fecf39

[30] G. Pepe and A. Carcaterra, "Semi-active damping by variational control algorithms," in *Proceedings of the International Conference on Structural Dynamic , EURODYN*, 2014, vol. 2014-January, pp. 1721-1727. [Online]. Available: https://www.scopus.com/inward/record.uri?eid=2-s2.0-84994438016&partnerID=40&md5=a1eee56015fd2beb9803f75b2215160c

[31] D. Antonelli, L. Nesi, G. Pepe, and A. Carcaterra, "Mechatronic control of the car response based on VFC," in *Proceedings of ISMA 2018 - International Conference on Noise and Vibration Engineering and USD 2018 - International Conference on Uncertainty in Structural Dynamics*, 2018, pp. 79-92. [Online]. Available: https://www.scopus.com/inward/record.uri?eid=2-s2.0-85060373090&partnerID=40&md5=ec5b75ae9b9810199c512bef66e38b56

[32] G. Pepe, D. Antonelli, L. Nesi, and A. Carcaterra, "Flop: Feedback local optimality control of the inverse pendulum oscillations," in *Proceedings of ISMA 2018 - International Conference on Noise and Vibration Engineering and USD 2018 - International Conference on Uncertainty in Structural Dynamics*, 2018, pp. 93-106. [Online]. Available: https://www.scopus.com/inward/record.uri?eid=2-s2.0-85060389675&partnerID=40&md5=d29242dd2913e82530da27cdf6ac222a

[33] E. Paifelman, G. Pepe, and A. Carcaterra, "An optimal indirect control of underwater vehicle," *International Journal of Control*, pp. 1-15, 2019, doi: 10.1080/00207179.2019.1590737.

[34] D. Antonelli, L. Nesi, G. Pepe, and A. Carcaterra, "A novel approach in Optimal trajectory identification for Autonomous driving in racetrack," in *2019 18th European Control Conference, ECC 2019*, 2019, pp. 3267-3272, doi: 10.23919/ECC.2019.8795637. [Online]. Available: https://www.scopus.com/inward/record.uri?eid=2-s2.0-85071599660&doi=10.23919/ECC.2019.8795637&partnerID=40&md5=3a2ef5ec295b9fb6f45c809983b9261e

[35] R. A. Rojas and A. Carcaterra, "An approach to optimal semi-active control of vibration energy harvesting based on MEMS," *Mechanical Systems and Signal Processing*, Article vol. 107, pp. 291-316, 2018, doi: 10.1016/j.ymssp.2017.11.005.

[36] Midé. https://www.mide.com/ (accessed.

[37] S. Timoshenko, *Vibration Problems in Engineering - Scholar's Choice Edition*. Scholar's Choice, 2015.

[38] A. Erturk and D. J. Inman, *Piezoelectric Energy Harvesting*. Wiley, 2011.

[39] A. Doria, F. Moro, D. Desideri, A. Maschio, and Z. Zhang, "An Impulsive Method for the Analysis of Piezoelectric Energy Harvesters for Intelligent Tires," no. 50138, p. V003T01A025, 2016, doi: 10.1115/DETC2016-59105.

[40] E. Paifelman, G. Pepe, F. La Gala, and A. Carcaterra, "Control of fluctuations of a tethered unmanned-underwater-vehicle," in *Proceedings of ISMA 2018 - International Conference on Noise and Vibration Engineering and USD 2018 - International Conference on Uncertainty in Structural Dynamics*, 2018, pp. 241-251. [Online]. Available: https://www.scopus.com/inward/record.uri?eid=2-s2.0-85060396810&partnerID=40&md5=c05d3e8126be9cb8cf5d96cd3e144633

[41] G. Pepe and A. Carcaterra, "A new semi-active variational based damping control," in *MESA 2014 - 10th IEEE/ASME International Conference on Mechatronic and Embedded Systems and Applications, Conference Proceedings*, 2014. [Online]. Available: http://www.scopus.com/inward/record.url?eid=2-s2.0-84911969901&partnerID=40&md5=3611145674b6d640dae8ba6b918382fa

[42] G. Pepe and A. Carcaterra, "Semi-Active Damping by Variational Control Algorithms," presented at the Proceedings of the 9th International Conference on Structural Dynamics, EURODYN 2014, Porto, Portugal, 30 June - 2 July 2014, 2014. [Online]. Available: http://paginas.fe.up.pt/~eurodyn2014//CD/papers/240_MS09_ABS_1721.pdf.

[43] G. Pepe, A. Carcaterra, I. Giorgio, and D. Del Vescovo, "Variational Feedback Control for a nonlinear beam under an earthquake excitation," *Mathematics and Mechanics of Solids*, 2014, doi: 10.1177/1081286514562878.

[44] A. E. Bryson, *Applied Optimal Control: Optimization, Estimation and Control* (Halsted Press book'). Taylor & Francis, 1975.

[45] P. A. Vikhar, "Evolutionary algorithms: A critical review and its future prospects," in *2016 International Conference on Global Trends in Signal Processing, Information Computing and Communication (ICGTSPICC)*, 22-24 Dec. 2016 2016, pp. 261-265, doi: 10.1109/ICGTSPICC.2016.7955308.

[46] M. Bazghaleh, S. Grainger, and M. Mohammadzaheri, "A review of charge methods for driving piezoelectric actuators," *Journal of Intelligent Material Systems and Structures*, vol. 29, no. 10, pp. 2096-2104, 2018/06/01 2017, doi: 10.1177/1045389X17733330.

[47] G. L. C. M. Abreu, J. F. Ribeiro, and V. Steffen Jr, "Experiments on optimal vibration control of a flexible beam containing piezoelectric sensors and actuators," *Shock and Vibration*, Article vol. 10, no. 5-6, pp. 283-300, 2003.

[48] E. Lu, W. Li, X. Yang, M. Fan, and Y. Liu, "Modelling and Composite Control of Single Flexible Manipulators with Piezoelectric Actuators," *Shock and Vibration*, Article vol. 2016, 2016, Art no. 2689178, doi: 10.1155/2016/2689178.

[49] X. Zhang, Z. Dong, C. Faria, K. Hengster-Movric, and W. Desmet, "Observer-Based Distributed Controllers Design for a Cantilever Beam," in *Sensors and Instrumentation, Volume 5*, Cham, E. Wee Sit, Ed., 2016// 2016: Springer International Publishing, pp. 163-170.

[50] R. Vatankhah, F. Karami, and H. Salarieh, "Observer-based vibration control of non-classical microcantilevers using extended Kalman filters," *Applied Mathematical Modelling*, vol. 39, no. 19, pp. 5986-5996, 2015/10/01/ 2015, doi: https://doi.org/10.1016/j.apm.2015.01.047.